Suppression of the Contrast of Ribs in Chest Radiographs by Means of Massive Training Artificial Neural Network

Kenji Suzuki, Hiroyuki Abe, Feng Li, Kunio Doi

Department of Radiology, The University of Chicago, Chicago, IL 60637

ABSTRACT

We developed a method for suppression of the contrast of ribs in chest radiographs by means of a massive training artificial neural network (MTANN). The MTANN is a trainable highly nonlinear filter that can be trained by using input chest radiographs and the corresponding teacher images. We used either the soft-tissue image or the bone image obtained by use of a dual-energy subtraction technique as the teacher image for suppression of ribs in chest radiographs. When the soft-tissue images were used as the teacher images, the MTANN directly produced a "soft-tissue-image-like" image where the contrast of ribs was suppressed. When the bone images were used as the teacher images, the MTANN was able to produce a "bone-image-like" image, and then was subtracted from the corresponding chest radiograph to produce a bone-subtracted image where ribs are suppressed. Thus, the two kinds of rib-suppressed images, i.e., the soft-tissue-image-like image and the bone-subtracted image, could be produced by use of the MTANNs trained with two different teacher images. We applied each of the two trained MTANNs to non-training chest radiographs to investigate the difference between the processed images. The results showed that the contrast of ribs in chest radiographs almost disappeared, and was reduced to less than 10% in both processed images. The contrast of ribs was reduced slightly better in the soft-tissue-image-like images than in the bone-subtracted images, whereas soft-tissue opacities such as lung vessels and nodules were maintained better in the bone-subtracted images. Therefore, the use of the bone images as the teacher images for training the MTANN has produced better rib-suppressed images where soft-tissue opacities were substantially maintained. A method for rib suppression using the MTANN would be useful for radiologists as well as CAD schemes in detection of lung diseases such as nodules in chest radiographs.

Keywords: dual-energy subtraction, computer-aided diagnosis (CAD), lung nodule, chest radiography, rib suppression

1. INTRODUCTION

Chest radiography has been used to detect lung cancer in screening programs,[1,2] because some evidence suggests that early detection of lung cancer may allow a favorable prognosis for the patient.[3-5] Radiologists, however, may fail to detect lung nodules in chest radiographs in up to 30% of cases[6,7] due to the overlap with normal anatomic structures such as ribs and clavicles.[8,9] Therefore, a computer-aided diagnostic (CAD) scheme for nodule detection on chest radiographs has been investigated as a useful tool, because the computer prompt for indicating nodules would improve radiologists' detection accuracy.[10,11]

Many researchers have developed CAD schemes for lung nodule detection in chest radiography.[12-19] Giger et al. developed a CAD scheme for nodule detection on chest radiographs,[12] and the performance of the CAD scheme was improved by incorporating an adaptive thresholding technique and a multiple-template matching technique by Xu et al.[13] and Li et al.[14], respectively. A major difficulty in current CAD schemes for chest radiographs is to detect nodules overlapping with ribs, rib crossings, and clavicles, because a majority of false positives were caused by ribs and clavicles.[13] This results in lowering the sensitivity of a CAD scheme as well as the specificity. Because the nodules overlapping with ribs and clavicles were reported to be difficult for radiologists,[8,9] detection of such nodules is important for a CAD scheme. Therefore, the suppression of ribs in chest radiographs would be useful for improving radiologists' detection accuracy and the CAD performance.

Our purpose in this study was to develop a method for suppression of the contrast of ribs in chest radiographs by means of a massive training artificial neural network (MTANN).

Medical Imaging 2004: Image Processing, edited by J. Michael Fitzpatrick, Milan Sonka, Proceedings of SPIE Vol. 5370 (SPIE, Bellingham, WA, 2004)
1605-7422/04/$15 doi: 10.1117/12.536436

2. MATERIALS

To train the MTANN and validate the results, we used dual-energy chest radiographs consisting of 128 conventional chest radiographs and the corresponding soft tissue images and bone images. The dual-energy chest radiographs were acquired with a computed radiography system with dual-energy subtraction (FCR 9501 ES; Fuji Medical Systems) at The University of Chicago Hospitals. One hundred eighteen of 128 chest radiographs were cases with solitary pulmonary nodules, and ten radiographs were "normal" cases (i.e., nodule-free cases). All nodules were confirmed by use of CT examinations. The original matrix size of the images was 1,760 x 1,760 pixels (pixel size was 0.2 mm), and the gray scale was 10 bit. For efficiency, the size of all images was reduced to 440 x 440 pixels in this study.

3. METHODS

3.1 Architecture of Massive Training Artificial Neural Network (MTANN)

Suzuki et al. have been investigating supervised nonlinear image-processing techniques based on artificial neural networks (ANNs), called a "neural filter"[20] for reduction of the quantum mottle in X-ray images[21] and a "neural edge detector"[22,23] for supervised detection of subjective edges traced by cardiologists,[24] and have developed training methods,[25,26] design methods,[27,28] and an analysis method[29] for these techniques. Suzuki et al. have recently extended the neural filter and the neural edge detector to accommodate various pattern-classification tasks, and developed an MTANN. They have applied the MTANN for reduction of false positives in computerized detection of lung nodules in low-dose CT.[30,31]

The MTANN is a trainable highly nonlinear filter that can be trained by using input chest radiographs and the corresponding teacher images. The MTANN consists of a modified multilayer ANN, which is capable of operating on image data directly. The pixel values of the original chest radiographs are normalized first such that a pixel value of zero is zero and a pixel value of 1,023 is one. The inputs of the MTANN are the pixel values in a local window R_S on a chest radiograph. The output of the MTANN is a continuous value, which corresponds to the center pixel in the local window, represented by

$$O(x,y) = NN\{g(x-i, y-j) \mid i, j \in R_S\}, \tag{1}$$

where $O(x,y)$ is the output of the MTANN, x and y are the indices of coordinates, $NN\{\bullet\}$ is the output of the modified multilayer ANN, and $g(x,y)$ is an input pixel value. Note that only one unit is employed in the output layer. The output image is obtained by scanning of an input image with the MTANN.

The teacher image is a desired image for suppressing ribs in a chest radiograph. The input chest radiograph is divided pixel-by-pixel into a large number of overlapping sub-regions. The size of the sub-region corresponds to that of the local window R_S. The MTANN is trained by presenting each of the input sub-regions together with each of the corresponding teacher single pixels. The error to be minimized by training is defined by

$$E = \frac{1}{2P}\sum_{p}\left\{T^{(p)} - O^{(p)}\right\}^2, \tag{2}$$

where p is a training pixel number, $T^{(p)}$ is the pth training pixel in the training regions R_T in the teacher images, $O^{(p)}$ is the pth training pixel in the training region R_T in the output images, and P is the number of training pixels. The MTANN is trained by a modified back-propagation (BP) algorithm,[32] which was derived for the structure of the modified multilayer ANN in the same way as the original BP algorithm.[33,34]

3.2 Multi-Resolution MTANN for Suppression of Ribs

Ribs in chest radiographs include various spatial frequency components. For a single-MTANN, it is difficult to suppress ribs containing such various frequencies, because the capability of a single MTANN is limited, i.e., the capability depends on the size of the local window of the MTANN. In order to overcome this issue, we employed a multi-resolution decomposition/composition technique.[35,36] The multi-resolution decomposition technique is a technique for decomposing an original high-resolution image into different-resolution images. First, a medium resolution image is obtained from the original high resolution image by performing down-sampling with averaging. The medium resolution image is enlarged by performing up-sampling with zeroth order holding. Then, a high resolution difference image is obtained by subtracting the enlarged medium resolution image from the high resolution image. These procedures are performed repeatedly to produce further lower resolution images. Thus, multi-resolution images having various frequencies are obtained by use of the multi-resolution decomposition technique. The important property of this technique is that exactly the same original resolution image can be obtained from the multi-resolution images by performing the inverse procedures, which are called a multi-resolution composition technique.

We used a dual-energy subtraction technique[37] to obtain the teacher images for suppression of ribs in chest radiographs. The dual-energy subtraction is a technique for obtaining a soft-tissue image and a bone image by use of the energy dependence of x-ray attenuation by different materials. Chest radiographs are used as input images to the MTANN, and the corresponding soft-tissue images or bone images are used as the teacher images for suppression of ribs in chest radiographs. We employed the multi-resolution decomposition and composition techniques, and developed a multi-resolution MTANN consisting of three MTANNs for three different-resolution images, as illustrated in Fig. 1. Each MTANN is an expert for a certain resolution such as a low-, a medium-, or a high-resolution. First, the input chest radiographs and the corresponding teacher images are decomposed into sets of different-resolution images, and then these sets of images are used for training the MTANNs in the multi-resolution MTANN. Each resolution MTANN is trained independently with the corresponding resolution images. After training, the MTANNs are expected to be able to produce different-resolution images. The different resolution output images are composed to provide a complete high resolution image by use of the multi-resolution composition technique.

When the soft-tissue image is used as the teacher image, the MTANN can directly produce a "soft-tissue-image-like" image where the contrast of ribs is suppressed. However, when the bone image is used as the teacher image, the MTANN can produce a "bone-image-like" image, and then is subtracted from the corresponding chest radiograph to produce a bone-subtracted image where ribs are suppressed. Thus, two kinds of rib-suppressed images, i.e., the soft-tissue-image-like image and the bone-subtracted image, can be produced by use of the MTANNs trained with two different teacher images. Therefore, this image processing may be considered as a "rib suppression" technique. Figure 2 shows a scheme for creating the bone-subtracted image from the “bone-image-like” image. To reduce the fine structures of soft tissues in the bone-image-like image, a Gaussian filter with a small standard deviation is applied to the bone-image-like image. To suppress only ribs, the image for masking the outside regions of the lung regions is created from the original chest radiograph by a method described below. Thresholding is performed on the chest radiograph to segment lung regions. The threshold value is determined by use of Otsu's threshold selection.[38] Otsu's threshold selection is a technique for determining a threshold from a histogram. This method selects the lowest point between two classes in the histogram automatically (it is formulated as linear discriminant analysis). The method involves minimizing the ratios of between-class variance to the total variance. A Gaussian filter with a standard deviation of 40 pixels was applied for smoothing the edges of the segmented lung region. The smoothed bone-image-like image of the multi-resolution MTANN is subtracted from the corresponding chest radiograph with the mask image.

4. RESULTS

4.1 Training with Soft-Tissue Images or Bone Images

We used four chest radiographs and the corresponding soft-tissue images and bone images from our dual-energy chest radiograph database for training the multi-resolution MTANN. One of important characteristics of the MTANN is that it can be trained with a very small number of cases, because the MTANN is trained with a large number of sub-regions extracted from input images, i.e., the MTANN can be trained not on case base but on sub-region base.[30,31] We used one typical normal case and three cases with nodules as training cases. Figure 3 shows a sample of the training cases. The normal case was used mainly for training for ribs, clavicles, soft tissues such as lung vessels, and the relationship among them. The nodule cases were used mainly for training for nodules and the relationship between nodules and ribs. In order to train the entire features in lung regions, 5,000 pairs of training samples were extracted randomly from manually-traced lung regions in each of different resolution normal chest radiographs and each of the corresponding teacher images. In order to learn the relationship between nodules and ribs, training samples for nodules were extracted from the manually-traced nodule regions which were enough to cover the nodules.

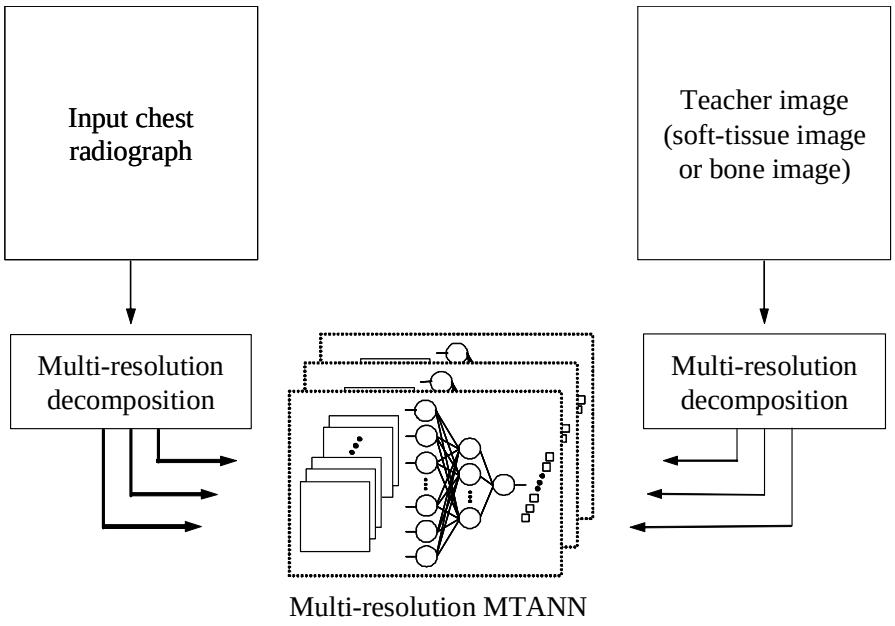

Figure 1. Architecture and training of the multi-resolution MTANN consisting of three MTANNs for three different-resolution images. The input chest radiograph and the teacher image are decomposed into multi-resolution images. Each of multi-resolution images is used as the input and teacher images for each of the corresponding resolution MTANN in the multi-resolution MTANN.

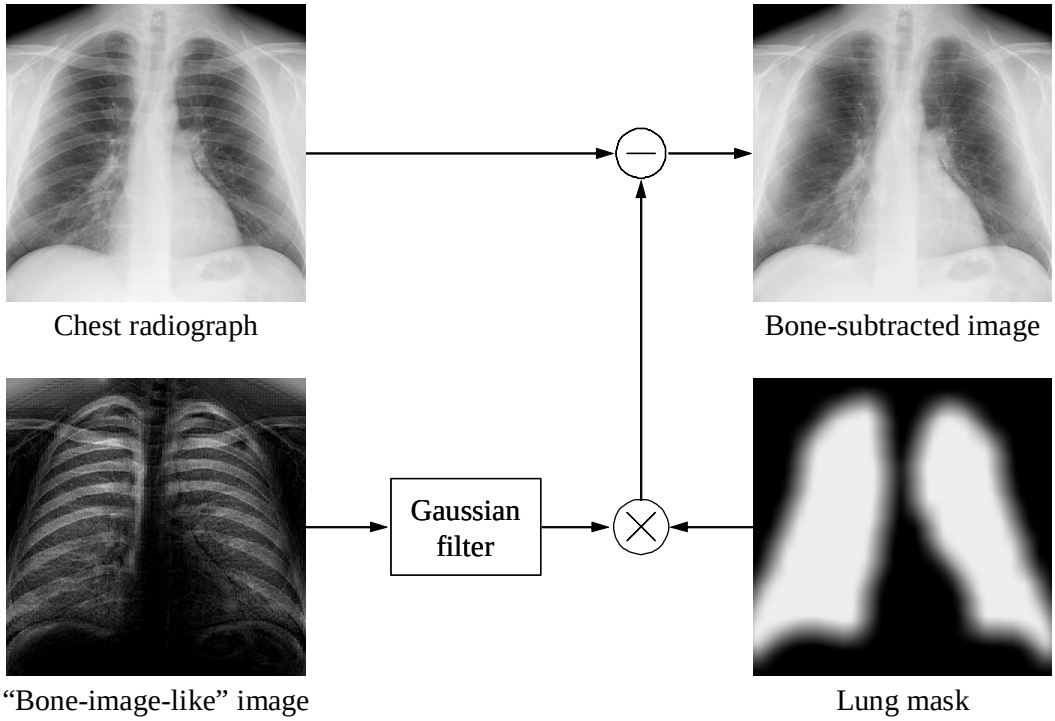

Figure 2. Illustration of a scheme for creating a bone-subtracted image from the "bone-image-like" image obtained by use of the trained MTANN.

We determined the size R_S of the local window of the MTANNs in the multi-resolution MTANN by using a method for designing the structure of an ANN.[27] The method is a sensitivity-based pruning method, i.e., the sensitivity to the training error was calculated when a certain unit was removed virtually, and the unit with the minimum training error was removed. Removing the redundant units in the input layer and retraining for recovering the potential loss due to the removal were performed repeatedly, resulting in a reduced structure where redundant units were removed. As a result, the size of the local window was determined to be 9 x 9 pixels. A three-layer structure was employed for the structure of the MTANNs, because any continuous mapping can be realized approximately by three-layer ANNs.[39,40] The number of hidden units was determined empirically to be 20; thus, the numbers of input, hidden, and output units were 81, 20, and 1, respectively. With the parameters above, the trainings of three MTANNs were performed 1,000,000 times. After training, the output images of the MTANNs were composed into an output image by use of the multi-resolution composition technique.

(a)

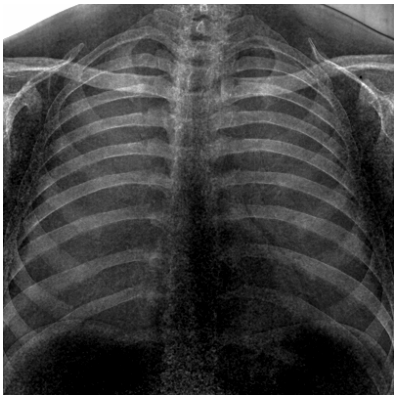

(b)

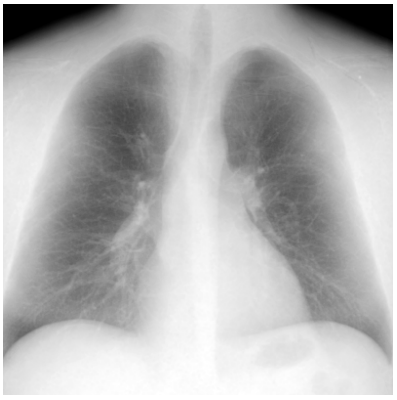

(c)

Figure 3. Illustrations of the training case (normal case) of (a) input chest radiograph, (b) corresponding teacher bone image, and (c) corresponding teacher soft-tissue image.

4.2 Comparison of the MTANNs Trained with Different Teacher Images

Figure 4 shows the output images, i.e., the soft-tissue-image-like image and the bone-image-like image, of the MTANNs with two different teacher images, and the bone-subtracted image for the chest radiograph in Fig. 3. In the soft-tissue-image-like image, the opacities of ribs almost disappear. In the bone-image-like image, the ribs are extracted effectively, and the image is similar to the "ideal" bone image in Fig. 3(c). In the bone-subtracted image, the contrast of ribs is suppressed substantially, while the visibility of soft tissue such as lung vessels is maintained. For detailed comparison of these images, enlarged images of regions-or-interest (ROIs) in the soft-tissue-image-like image and the rib-subtracted image are shown in Fig. 5. Compared to the "ideal" soft-tissue image, details of soft tissue such as very small lung vessels slightly disappear in the soft-tissue-image-like image, whereas they are maintained substantially in the bone-subtracted image, although low-contrast ribs are recognizable. Figures 6 and 8 show the output images of the MTANNs for a non-training normal case and a non-training case with a nodule, respectively. Figures 7 and 9 show the enlarged images of ROIs in these images. The results demonstrated that the MTANN worked similar for non-training cases. As to the nodule case, the nodule in the bone-subtracted image shown in Fig. 9 is maintained substantially, it is similar to the "ideal" soft-tissue image. The effect of the rib suppression was evaluated by measuring the contrast of ribs in both original chest radiographs and processed images. The contrast of the 6th left and right ribs, and that of the 9th left and right ribs was measured. The results demonstrated that the contrast of ribs in chest radiographs was reduced to about 6% in the soft-tissue-image-like images, and about 8% in the bone-subtracted images.

The MTANN trained with the bone images produced better results compared to the MTANN trained with the soft-tissue images, probably because the pattern variations of soft tissue would be greater than those of ribs. Another advantage of the bone-subtracted image is that different contrast of ribs can be obtained by changing a weighting factor.

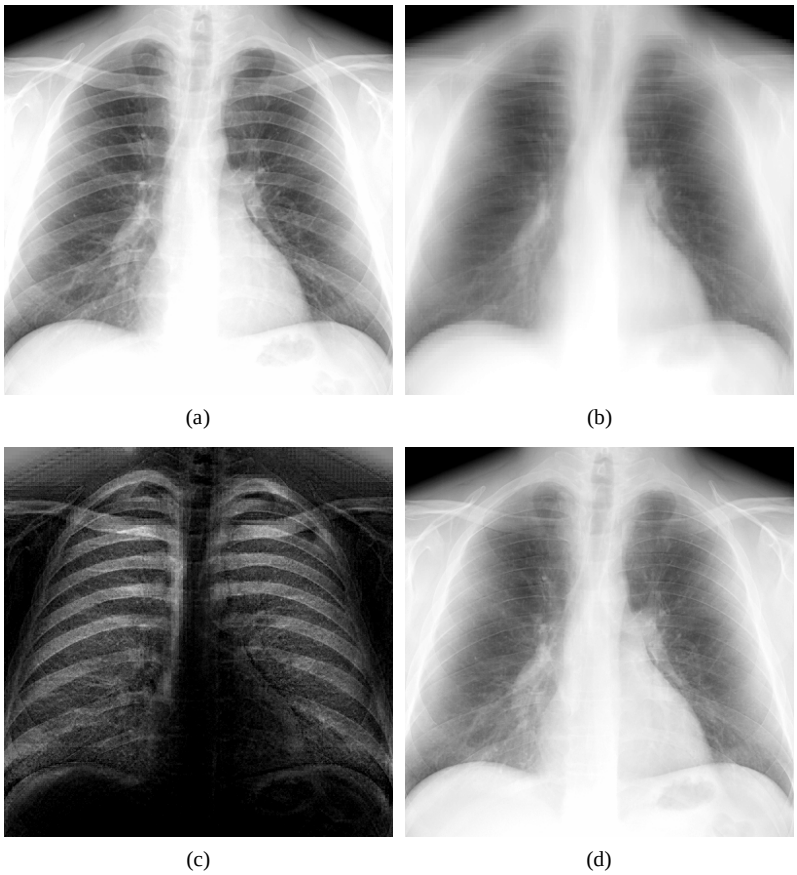

Figure 4. Illustrations of (a) original chest radiograph, (b) "soft-tissue-image-like" image obtained by use of the MTANN, (c) "bone-image-like" image obtained by use of the MTANN, and (d) bone-subtracted image obtained by subtracting the bone-image-like image from the original chest radiograph, which correspond to the chest radiographs in Fig. 3

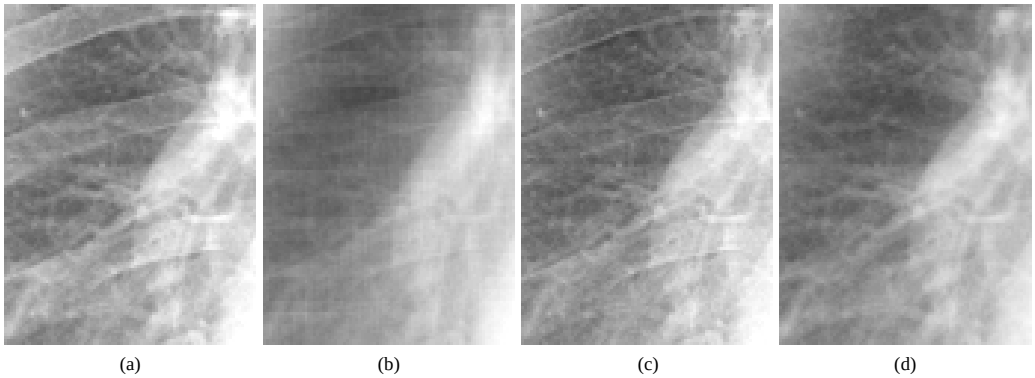

Figure 5. Enlarged images of regions-or-interest (ROIs) in (a) original chest radiograph, (b) "soft-tissue-image-like" image obtained by use of the MTANN, (c) bone-subtracted image obtained by use of our scheme, and (d) "ideal" soft-tissue image obtained by use of the dual-energy subtraction technique.

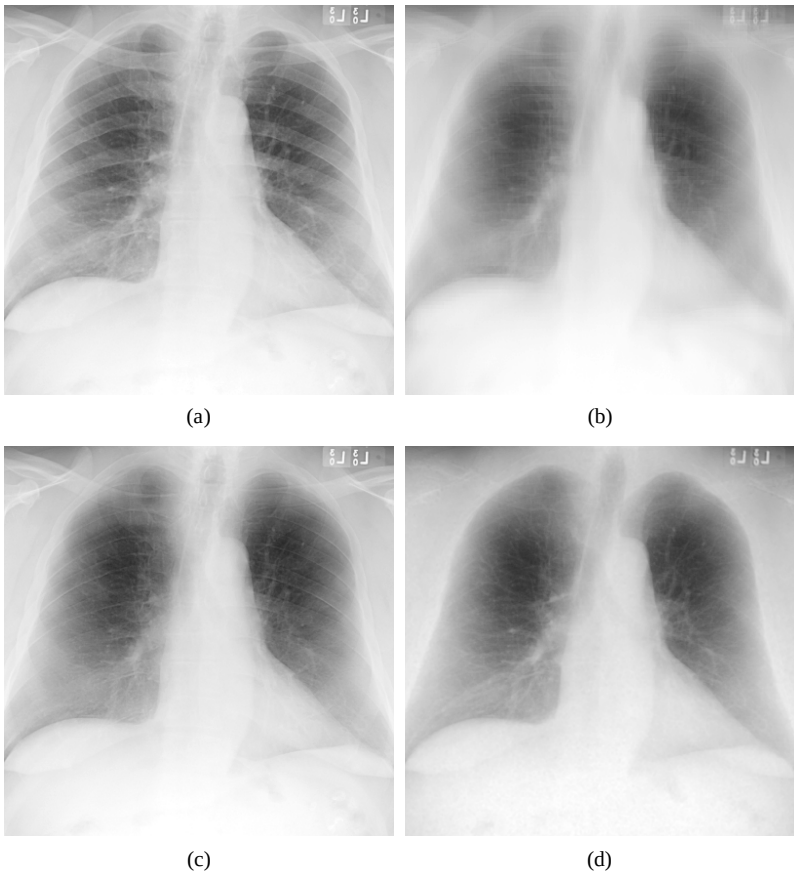

(a) (b)

(c) (d)

Figure 6. Illustrations of a non-training normal case of (a) original chest radiograph, (b) "soft-tissue-image-like" image obtained by use of the MTANN, (c) bone-subtracted image obtained by use of our scheme, and (d) "ideal" soft-tissue image obtained by use of the dual-energy subtraction technique.

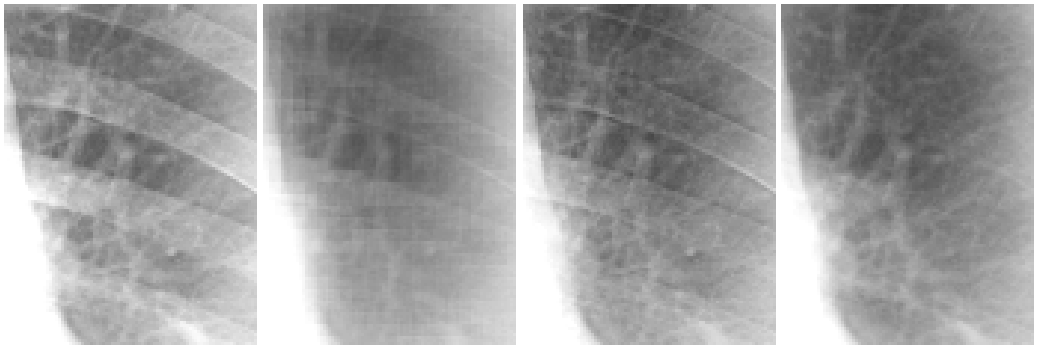

(a) (b) (c) (d)

Figure 7. Enlarged images of ROIs in (a) original chest radiograph, (b) "soft-tissue-image-like" image obtained by use of the MTANN, (c) bone-subtracted image obtained by use of our scheme, and (d) "ideal" soft-tissue image obtained by use of the dual-energy subtraction technique.

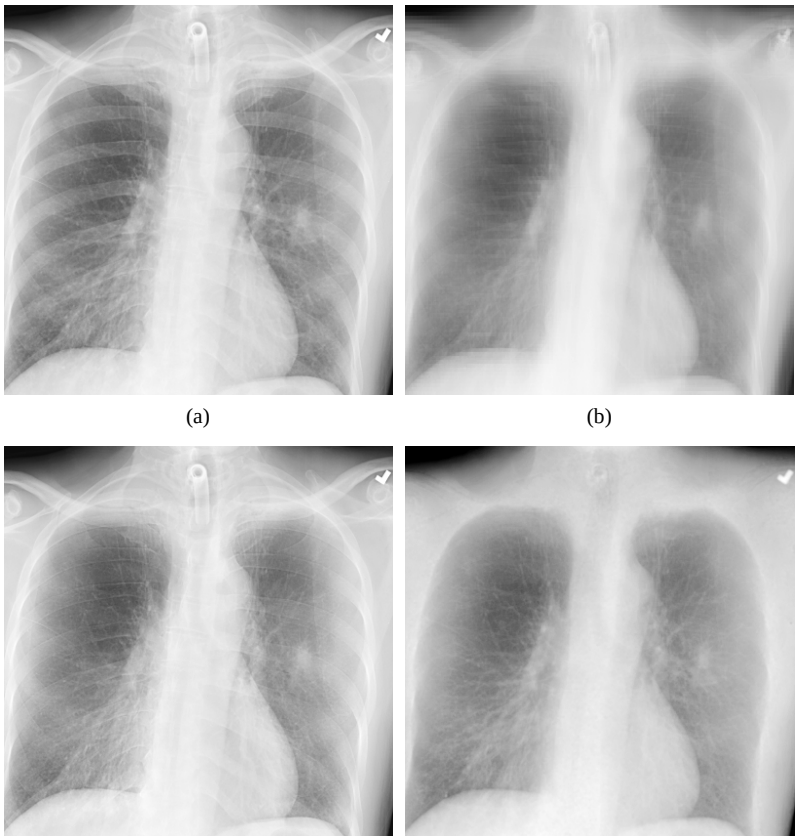

(a) (b)

(c) (d)

Figure 8. Illustrations of a non-training case with a nodule of (a) original chest radiograph with a nodule (in the left lung), (b) "soft-tissue-image-like" image obtained by use of the MTANN, (c) bone-subtracted image obtained by use of our scheme, and (d) "ideal" soft-tissue image obtained by use of the dual-energy subtraction technique.

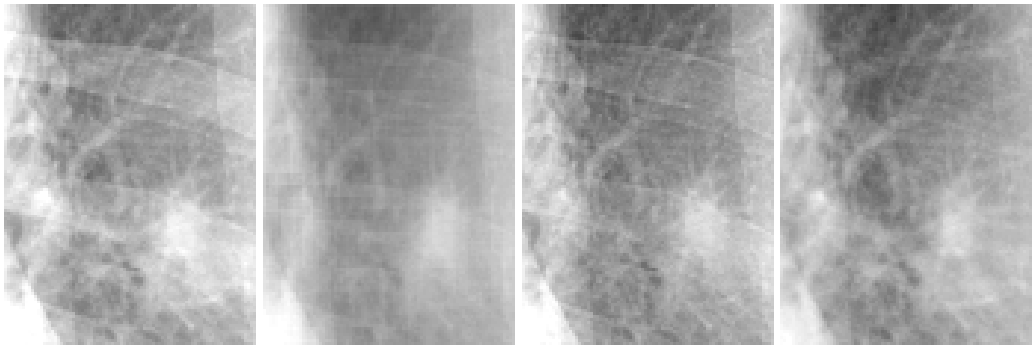

(a) (b) (c) (d)

Figure 9. Enlarged images of ROIs of a nodule in (a) original chest radiograph, (b) "soft-tissue-image-like" image obtained by use of the MTANN, (c) bone-subtracted image obtained by use of our scheme, and (d) "ideal" soft-tissue image obtained by use of the dual-energy subtraction technique.

6. CONCLUSION

The use of the bone images as the teacher images for training the MTANN produced better rib-suppressed images where the soft-tissue opacities were substantially maintained. A method for rib suppression using the MTANN would be useful for radiologists as well as CAD schemes in detecting lung diseases such as nodules in chest radiographs.

7. ACKNOWLEDGMENTS

The authors are grateful to Junji Shiraishi, PhD, for his valuable suggestions, Heber MacMahon, MD, for his clinical advice, and Qiang Li, PhD, Hidetaka Arimura, PhD, Hotaka Takizawa, PhD, Roger Engelmann, MS, and Chisako Muramatsu, BA, for their valuable suggestions. This work was supported by USPHS Grant No. CA62625. K. Doi is a shareholder in R2 Technology, Inc., Sunnyvale, CA, and Deus Technologies, Inc., Rockville, MD. It is the policy of the University of Chicago that investigators disclose publicly actual or potential significant financial interest that may appear to be affected by research activities.

8. REFERENCES

1. Kubik A, Polak J. Lung cancer detection: results of a randomized prospective study in Czechoslovakia. *Cancer* 57: 2427-2437, 1986.
2. Henschke CI, Miettinen OS, Yankelevitz DF, Libby DM, Smith JP. Radiographic screening for cancer: proposed paradigm for requisite research. *Clinical Imaging* 18: 16-20, 1994.
3. Flehinger BJ, Kimmel M, Melamed MR. The effect of surgical treatment on survival from early lung cancer: implication for screening. *Chest* 101: 1013-1018, 1992.
4. Sobue T, Suzuki R, Matsuda M, Kuroishi T, Ikeda S, Naruke T. Survival for clinical stage I lung cancer not surgically treated. *Cancer* 69: 685-692, 1992.
5. Heelan RT, Flehinger BJ, Melamed MR, Zaman MB, Perchick WB, Caravelli JF, Martini N. Non-small-cell lung cancer: results of the New York screening program. *Radiology* 151: 289-293, 1984.
6. Austin JHM, Romney BM, Goldsmith LS. Missed bronchogenic carcinoma: radiographic findings in 27 patients with a potentially resectable lesion evident in retrospect. *Radiology* 182: 115-122, 1992.
7. Shah PK, Austin JHM, White CS, Patel P, Haramati LB, Pearson GDN, Shiau MC, Berkmen YM. Missed non-small cell lung cancer: radiographic findings of potentially resectable lesions evident only in retrospect. *Radiology* 226: 235-241, 2003.
8. Kelcz F, Zink FE, Peppler WW, Kruger DG, Ergun DL, Mistretta CA Conventional chest radiography vs dual-energy computed radiography in the detection and characterization of pulmonary nodules. *AJR* 162: 271-278, 1994.
9. Ergun DL, Mistretta CA, Brown DB, Bystrianyk RT, Kwong Sze W, Kelcz F, Naidich DR. Single-exposure dual-energy computed radiography: improved detection and processing. *Radiology*. 174: 243-249, 1990.
10. Abe K, Doi K, MacMahon H, Giger ML, Jia H, Chen X, Kano A, Yanagisawa T: Computer-aided diagnosis in chest radiography: analysis of results in a large clinical series. *Invest Radiol* 28: 987-993, 1993.
11. Kobayashi T, Xu XW, MacMahon H, Metz CE, Doi K. Effect of a computer-aided diagnosis scheme on radiologists' performance in detection of lung nodules on radiographs. *Radiology* 199: 843-848, 1996.
12. Giger ML, Doi K, MacMahon H. Image feature analysis and computer-aided diagnosis in digital radiography. 3. Automated detection of nodules in peripheral lung fields. *Med Phys* 15: 158-166, 1988.
13. Xu XW, Doi K, Kobayashi T, MacMahon H, Giger ML. Development of an improved CAD scheme for automated detection of lung nodules in digital chest images. *Med Phys* 24: 1395-1403, 1997.
14. Li Q, Katsuragawa S, Doi K. Computer-aided diagnostic scheme for pulmonary nodule detection in digital chest radiographs: elimination of false-positives by using a multiple-templates matching technique. *Med Phys* 28: 2070-2076, 2001.
15. Ballard D, Sklansky J. A ladder-structured decision tree for recognizing tumors in chest radiographs. *IEEE Trans Computer* 20: 503-513, 1976.

16. Lo SC, Lou Sl, Lin JS, Freedman M, Chien M, Mun S. Artificial convolution neural network techniques and applications for lung nodule detection. *IEEE Trans Med Imag* 14: 711-718, 1995.
17. Lin JS, Lo SC, Hasegawa A, Freedman M, Mun S. Reduction of false positives in lung nodule detection using a two–level neural classification. *IEEE Trans Med Imag* 15: 206-217, 1996.
18. Carreira MJ, Cabello D, Penedo MG, Mosquera A. Computer-aided diagnosis: automatic detection of lung nodules. *Med Phys* 25: 1998-2006, 1998.
19. Penedo MG, Carreira MJ, Mosquera A, Cabello D. Computer-aided diagnosis: a neural-network-based approach to lung nodule detection. *IEEE Trans Med Imag* 17: 872-880, 1998.
20. Suzuki K, Horiba I, Sugie N, Nanki M. Noise reduction of medical X-ray image sequences using a neural filter with spatiotemporal inputs. *Proc Int Symp Noise Reduction for Imag and Comm Systems* 85-90, 1998.
21. Suzuki K, Horiba I, Sugie N, Nanki M. Neural filter with selection of input features and its application to image quality improvement of medical image sequences. *IEICE Trans Information and Systems* E85-D: 1710-1718, 2002.
22. Suzuki K, Horiba I, Sugie N. Neural edge detector -a good mimic of conventional one yet robuster against noise. *Lecture Notes in Computer Science* 2085: 303-310, 2001.
23. Suzuki K, Horiba I, Sugie N. Neural edge enhancer for supervised edge enhancement from noisy images. *IEEE Trans Pattern Analysis and Machine Intelligence* 25: 1582-1596, 2003.
24. Suzuki K, Horiba I, Sugie N, Nanki M. Extraction of left ventricular contours from left ventriculograms by means of a neural edge detector. *IEEE Trans on Medical Imaging* 23, 2004 (in press).
25. Suzuki K, Horiba I, Sugie N. Training under achievement quotient criterion. *IEEE Neural Networks for Signal Processing* X 537-546, 2000.
26. Suzuki K, Horiba I, Sugie N. Simple unit-pruning with gain-changing training. *IEEE Neural Networks for Signal Processing* XI 153-162, 2001
27. Suzuki K, Horiba I, Sugie N. Designing the optimal structure of a neural filter. *IEEE Neural Networks for Signal Processing* VIII 323-332, 1998.
28. Suzuki K, Horiba I, Sugie N. A simple neural network pruning algorithm with application to filter synthesis. *Neural Processing Letters* 13: 43-53, 2001.
29. Suzuki K, Horiba I, Sugie N. Efficient approximation of a neural filter for quantum noise removal in X-ray images. *IEEE Trans Signal Processing* 50: 1787-1799, 2002.
30. Suzuki K, Armato III S. G, Li F, Sone S, Doi K. Massive training artificial neural network (MTANN) for reduction of false positives in computerized detection of lung nodules in low-dose CT. *Medical Physics*, vol. 30, no. 7, pp. 1602-1617, July 2003.
31. Suzuki K, Armato III S. G, Li F, Sone S, Doi K. Effect of a small number of training cases on the performance of massive training artificial neural network (MTANN) for reduction of false positives in computerized detection of lung nodules in low-dose CT. *Proc. SPIE Medical Imaging (SPIE MI)* 5032: 1355-1366, 2003.
32. Suzuki K, Horiba I, Ikegaya K, Nanki M. Recognition of coronary arterial stenosis using neural network on DSA system. *Systems and Computers in Japan* 26: 66-74, 1995.
33. Rumelhart DE, Hinton GE, Williams RJ. Learning representations of back-propagation errors. *Nature* 323: 533-536, 1986.
34. Rumelhart DE, Hinton GE, Williams RJ. Learning internal representations by error propagation. *Parallel Distributed Processing* (MIT Press, Cambridge), 1: 318-362, 1986.
35. GM Stephane. A theory for multiresolution signal decomposition: the wavelet representation. *IEEE Trans Pattern Analysis and Machine Intelligence* 11:674-693, 1989.
36. Akansu AN, Haddad RA. *Multiresolution Signal Decomposition* (Academic Press), 1992.
37. Oestman JW, Greene R, Rhea JT et al. Single exposure dual energy digital radiography in the detection of pulmonary nodules and calcifications. *Invest Radiol* 24: 517-521, 1989.
38. Otsu N. A threshold selection method from gray-level histograms. *IEEE Trans Systems, Man and Cybernetics* 9: 62-66, 1979.
39. Funahashi K. On the approximate realization of continuous mappings by neural networks. *Neural Networks* 2: 183-192, 1989.
40. Barron AR. Universal approximation bounds for superpositions of a sigmoidal function. *IEEE Trans Information Theory* 39: 930-945, 1993.